

# Novel Pairing State in $\text{Cu}_x\text{Bi}_2\text{Se}_3$ Superconductor Probed by the Superfluid Density

M. Kriener, Kouji Segawa, Satoshi Sasaki, and Yoichi Ando

*Institute of Scientific and Industrial Research, Ibaraki, Osaka University, Osaka 567-0047, Japan*

(Dated: December 3, 2024)

$\text{Cu}_x\text{Bi}_2\text{Se}_3$  was recently elucidated to be the first example of a time-reversal-invariant topological superconductor accompanied by helical Majorana fermions on the surface. Here we present that progressive Cu intercalation into this system introduces significant disorder and leads to an anomalous suppression of the superfluid density which was obtained from the measurements of the lower critical field. At the same time, the transition temperature  $T_c$  is only moderately suppressed, which agrees with a recent prediction for the impurity effect in this class of topological superconductors bearing strong spin-orbit coupling. Those unusual disorder effects give further support to the novel odd-parity pairing state in  $\text{Cu}_x\text{Bi}_2\text{Se}_3$ .

PACS numbers: 74.20.Mn; 74.20.Rp; 74.25.Bt; 74.62.Dh

A topological superconductor (TSC) is a superconducting analogue of topological insulators (TIs) and is characterized by a nontrivial topological structure of the Hilbert space, which is specified by nontrivial  $Z$  or  $Z_2$  topologies [1–7]. Its hallmark signature is the appearance of surface Majorana fermions, which are their own antiparticles and are of fundamental intellectual interest [8]. Recently, it was theoretically predicted [9] and experimentally confirmed [10] that a superconducting doped TI material  $\text{Cu}_x\text{Bi}_2\text{Se}_3$  is the first concrete example of a time-reversal-invariant TSC. Its parent TI material  $\text{Bi}_2\text{Se}_3$  consists of basic crystallographic units of Se–Bi–Se–Bi–Se quintuple layers, which are weakly bonded by the van der Waals force. Upon intercalation of Cu into the van der Waals gap, superconductivity appears below the critical temperature  $T_c$  of up to  $\sim 3.8$  K [11]. This is high for its low charge carrier concentration of only  $\sim 10^{20} \text{ cm}^{-3}$  [11]. As a “superconducting topological insulator”, this material has attracted a great deal of interest [9, 12–26].

Unfortunately,  $\text{Cu}_x\text{Bi}_2\text{Se}_3$  has a materials problem that samples with a large superconducting volume fraction are difficult to obtain with the usual melt-growth method [11, 12], which hindered detailed studies of the superconducting properties of this material. However, this problem has recently been ameliorated by the development of electrochemical synthesis technique [18] which allowed the synthesis of superconducting samples with the shielding fraction exceeding 50% [17]. Such an improvement made it possible to perform point-contact spectroscopy on a cleaved surface of  $\text{Cu}_x\text{Bi}_2\text{Se}_3$  to find clear signature of the Andreev bound state in the form of a pronounced zero-bias conductance peak [10], which gives strong evidence for unconventional superconductivity [27, 28]. Knowing that the symmetry of this material [29, 30] allows only four types of superconducting gap functions [9] and that all possible unconventional states are topological [10], it was possible to conclude that  $\text{Cu}_x\text{Bi}_2\text{Se}_3$  is a TSC [10].

Although the point-contact spectroscopy elucidated

the TSC nature of  $\text{Cu}_x\text{Bi}_2\text{Se}_3$ , the electron mean free path  $\ell$  in the superconducting samples of this material is comparable to the coherence length  $\xi_0$  [17]; according to the common belief [31, 32], the odd-parity pairing should be strongly suppressed by impurity scattering in such a situation [33, 34]. In this context, a recent theory by Michaeli and Fu addressed this issue [23] and showed that odd-parity superconductivity in strongly spin-orbit coupled semiconductors like  $\text{Cu}_x\text{Bi}_2\text{Se}_3$  are much more robust against the pair-breaking effect induced by impurity scattering than in more ordinary odd-parity superconductors. Therefore, thanks to the role of spin-orbit coupling,  $T_c$  of  $\text{Cu}_x\text{Bi}_2\text{Se}_3$  is expected to be rather insensitive to nonmagnetic impurities, similarly to conventional superconductors [35].

In this Letter, we address the issue of disorder effects in  $\text{Cu}_x\text{Bi}_2\text{Se}_3$ . Through our systematic studies of the effects of Cu intercalation in this system, it turned out that increasing the Cu content beyond  $x \sim 0.3$  in the superconducting regime does not increase  $T_c$  nor the carrier concentration, but its main effect is to enhance the residual resistivity  $\rho_0$ . This suggests that one can consider the Cu content  $x$  to be a parameter to control the disorder while keeping other fundamental parameters essentially unchanged. By looking at the data from this perspective, the  $x$  dependence of the superfluid density obtained from the lower critical field shows an unusual disorder dependence that is distinct from that in conventional BCS superconductors, which gives strong support to unconventional pairing. In addition, we show that the  $x$  dependence of  $T_c$  is essentially a reflection of the disorder effect and is consistent with the particular odd-parity pairing state that is supposed to be realized in  $\text{Cu}_x\text{Bi}_2\text{Se}_3$ .

$\text{Cu}_x\text{Bi}_2\text{Se}_3$  single crystals of slab-like geometry with various Cu contents  $0.11 \leq x \leq 0.50$  were prepared by the electrochemical technique described earlier [18]. The magnetic field dependence of the magnetization,  $M(B)$ , were measured with a commercial SQUID magnetometer (Quantum Design MPMS) with particular attention paid to the low field regime [36]. Roughly half of the samples

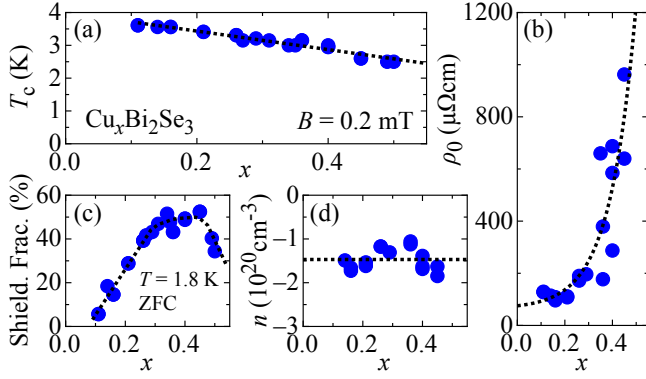


FIG. 1. (color online) Cu content  $x$  dependences of (a) critical temperature  $T_c$ , (b) residual resistivity  $\rho_0$ , (c) superconducting shielding fraction, and (d) normal-state carrier density  $n$ . Note that  $n$  is essentially  $x$  independent and remains low at  $\sim 1.5 \times 10^{20} \text{ cm}^{-3}$ . The dotted lines are guides to the eyes.

were also characterized by transport measurements by a standard six-probe method. Figure 1 summarizes the  $x$  dependences of  $T_c$ ,  $\rho_0$  (defined as  $\rho$  at  $T = 5$  K), the superconducting shielding fraction at  $T = 1.8$  K, and the charge carrier concentration  $n$  (determined from the Hall coefficient at 5 K). Most notably,  $\rho_0$  strongly increases for  $x > 0.3$  and  $n$  is basically independent of  $x$  at  $n \simeq 1.5 \times 10^{20} \text{ cm}^{-3}$ .

Before presenting magnetic properties, we define and summarize important parameters. The layered structure of  $\text{Cu}_x\text{Bi}_2\text{Se}_3$  leads to anisotropies in the superconducting parameters, and we denote the lower and upper critical fields for magnetic fields parallel and perpendicular to the crystallographic  $ab$  planes as  $B_{c1,ab}$ ,  $B_{c1,c}$ ,  $B_{c2,ab}$ , and  $B_{c2,c}$ , respectively. Also, the penetration depths and the coherence lengths along the in-plane and out-of-plane directions are denoted as  $\lambda_{ab}$ ,  $\lambda_c$ ,  $\xi_{ab}$ , and  $\xi_c$ , respectively. The anisotropic Ginzburg-Landau parameters are defined as  $\kappa_{ab} = \sqrt{\lambda_{ab}\lambda_c/(\xi_{ab}\xi_c)}$  and  $\kappa_c = \lambda_{ab}/\xi_{ab}$  [37–39]. The upper critical fields are related to the coherence lengths via  $B_{c2,ab} = \Phi_0/2\pi\xi_{ab}\xi_c$  and  $B_{c2,c} = \Phi_0/2\pi\xi_{ab}^2$  with the flux quantum  $\Phi_0$ . In the Ginzburg-Landau theory,  $B_{c1}$  is related to the vortex line energy  $E$  via  $B_{c1} = 4\pi\mu_0 E/\Phi_0$  [40]; for strongly type-II superconductors with  $\kappa \gg 1$ , one obtains  $E \approx [\Phi_0^2/(4\pi\lambda)^2] \ln \kappa$ . However, to take into account the vortex core energy, the  $\ln \kappa$  term has to be corrected by adding 0.5 [41–43], and the formula for  $B_{c1,ab}$  becomes

$$B_{c1,ab} = \frac{\Phi_0}{4\pi} [\ln(\kappa_{ab}) + 0.5] \frac{1}{\lambda_{ab}\lambda_c}. \quad (1)$$

Hence, to calculate the Ginzburg-Landau parameter  $\kappa_{ab}$ , we use  $B_{c1,ab}/B_{c2,ab} = (\ln \kappa_{ab} + 0.5)/2\kappa_{ab}^2$ . The anisotropy factor is defined as  $\gamma \equiv B_{c2,ab}/B_{c2,c} = B_{c1,c}/B_{c1,ab} = \lambda_c/\lambda_{ab}$  and the penetration depths are determined by solving Eq. 1 for  $\lambda_{ab}$  by using  $\lambda_c = \gamma\lambda_{ab}$ . For the following discussion, we define the averaged penetra-

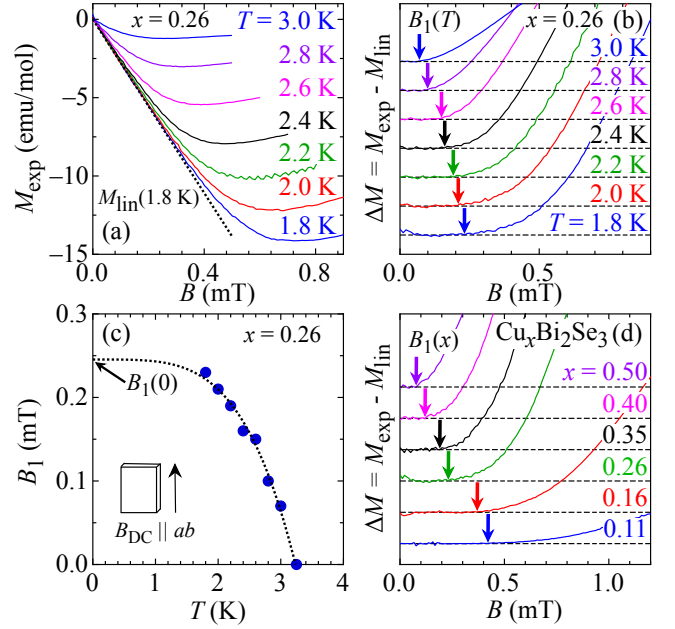


FIG. 2. (color online) (a) Initial low-field  $M_{\text{exp}}$  vs  $B$  curves for a sample with  $x = 0.26$  at various temperatures. (b) Reduced magnetization  $\Delta M$  after subtracting the initial linear Meissner contribution  $M_{\text{lin}}$ . The deviation points marked by arrows indicate  $B_1$  at each temperature. (c) Plot of  $B_1$  vs  $T$  for  $x = 0.26$  together with a fit to the data. (d) Plots of  $\Delta M$  vs  $B$  at 1.8 K for various  $x$ .

tion depth  $\lambda_{\text{av}} = \sqrt[3]{\lambda_{ab}^2\lambda_c}$ , which allows the calculation of the superfluid density via  $n_s = m^*/(\mu_0 e^2 \lambda_{\text{av}}^2)$  with the effective mass  $m^*$  assumed to be  $x$  independent [44].

Figure 2 describes how  $B_{c1,ab}$  is determined from the magnetization data  $M_{\text{exp}}$ , which is essentially the same as was done in Ref. [17]. Figure 2(a) shows  $M_{\text{exp}}(B)$  curves for a sample with  $x = 0.26$  at various temperatures between 1.8 and 3.0 K; the  $T_c$  of this sample was  $\sim 3.2$  K. The dashed line  $M_{\text{lin}}$  is a fit to the low-field magnetization at 1.8 K, representing the initial Meissner screening. Determining such a linear part for each temperature and subtracting it from the  $M_{\text{exp}}(B)$  data yields  $\Delta M = M_{\text{exp}} - M_{\text{lin}}$  which is shown in Fig. 2(b) (the data are shifted for clarity). The arrows mark the field  $B_1(T)$  at which the data start to deviate from zero, signaling the first flux entry into the sample. These data points are plotted as  $B_1$  vs  $T$  in Fig. 2(c) and are fitted with the empirical formula  $B_1(T) = B_1(0)[1 - (T/T_c)^4]$  [17]. Sometimes the  $B_1(T)$  data scatter around the fitting line, which leads to a sample-dependent error bar on  $B_1(0)$ . To show the trend of how  $B_1$  changes with the Cu concentration  $x$ , the 1.8-K magnetization data for various  $x$  are shown in Fig. 2(d); this plot clearly indicates that  $B_1(0)$  becomes systematically smaller for larger  $x$ .

From  $B_1(0)$  we calculate  $B_{c1}$  by taking into account the demagnetization effect due to the sample shape. Albeit small in the present case, this effect is

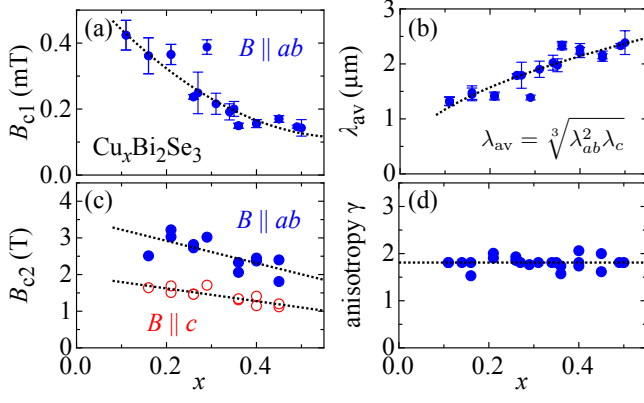


FIG. 3. (color online)  $x$  dependences of (a)  $B_{c1}(0)$  for  $B \parallel ab$  after the demagnetization correction, (b) corresponding penetration depth  $\lambda_{av}$ , (c)  $B_{c2}(0)$  for fields parallel and perpendicular to the  $ab$  planes, and (d) anisotropy factor  $\gamma$ . Dotted lines are guides to the eyes.

corrected for by employing Brandt's formula for slab-shaped samples with an aspect ratio  $b/a$  [45]:  $B_{c1}(0) = B_1(0)/\tanh\sqrt{0.36b/a}$ . The obtained  $B_{c1}$  for all samples are plotted vs  $x$  in Fig. 3(a). The corresponding  $\lambda_{av}$  values are shown in Fig. 3(b); for calculating  $\lambda_{av}$ , we need the anisotropy factor  $\gamma$  which was obtained from anisotropic  $B_{c2}$  determined from the resistive transitions in magnetic fields applied parallel and perpendicular to the  $ab$  plane [Fig. 3(c)]. The obtained  $\gamma$  is essentially independent of  $x$  [Fig. 3(d)], which supports the idea that the main effect of Cu intercalation beyond  $x \sim 0.3$  is to enhance the disorder without changing band structure or mobile carrier density.

As already mentioned, the averaged penetration depth  $\lambda_{av}$  directly gives the superfluid density  $n_s = m^*/(\mu_0 e^2 \lambda_{av}^2)$ . We normalize this value with the normal-state carrier density  $n$ , and Fig. 4(a) summarizes the  $x$  dependence of  $n_s^{\text{exp}} \equiv n_s/n$ . One can see that  $n_s/n$  is already only 0.3 at  $x \simeq 0.10$  where the superconductivity starts to appear, and it is further suppressed with increasing  $x$ . This behavior is obviously a reflection of strong disorder caused by Cu intercalation that can be inferred in Fig. 1(b). Since it is known that disorder causes a reduction in  $n_s$  even in conventional BCS superconductors [46, 47], it is prudent to discuss this behavior quantitatively.

According to the Anderson's theorem [35], the superconducting gap  $\Delta_0$  and  $T_c$  of conventional superconductors are relatively insensitive to small concentrations of nonmagnetic impurities. However, the superfluid density, which reflects the "rigidity" of the electronic system to electromagnetic perturbations, is affected by disorder in conventional superconductors [46–48]. Indeed, the disorder dependence of  $n_s$  has been studied in Nb and Pb and was found to follow the theoretical prediction [49, 50]. We therefore compare the disorder dependence of  $n_s$  ob-

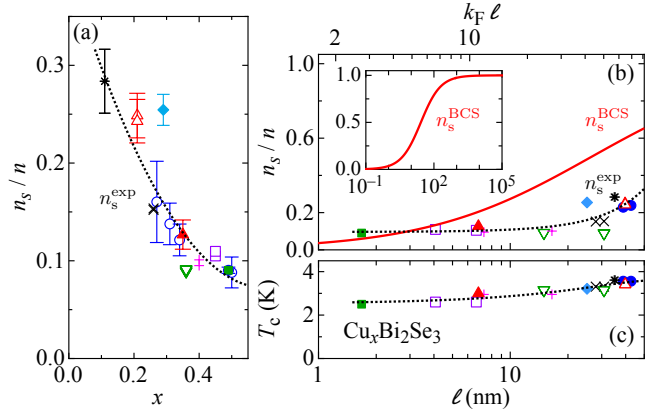


FIG. 4. (color online) (a) Normalized superfluid density  $n_s/n$  vs  $x$ , with  $n$  the normal-state carrier density. For symbols without error bars, the estimated errors are smaller than the symbol size. (b,c) Semi-log plots of  $n_s/n$  (b) and  $T_c$  (c) vs the mean-free path  $\ell$ . The upper axis gives the corresponding  $k_F \ell$  value. To facilitate comparisons between (a) and (b/c), data for different  $x$  values are indicated by different symbols. The solid line  $n_s^{\text{BCS}}$  in (b) gives the expected disorder-induced suppression of  $n_s/n$  for a conventional BCS superconductor. The inset shows  $n_s^{\text{BCS}} \rightarrow 1$  in the clean limit  $\ell \rightarrow \infty$ . The dotted lines in all panels are guides to the eyes.

served in  $\text{Cu}_x\text{Bi}_2\text{Se}_3$  to the expectation for ordinary BCS superconductors. For such a comparison, one needs to parameterize disorder, which is usually done by evaluating  $k_F \ell$ , where  $k_F = \sqrt{3\pi^2 n}$  is the Fermi wave number and  $\ell = \hbar k_F / (\rho_0 n e^2)$  is the mean free path [51].

For a pure BCS superconductor, the penetration depth in the 0-K limit is given by  $\lambda_L^2(0) = m^*/(\mu_0 e^2 n)$ , because  $n_s$  is equal to  $n$  in the clean limit. In the presence of disorder, this  $\lambda_L(0)$  in the clean limit is modified to an effective penetration depth which is evaluated at  $T = 0$  K as  $\lambda_{\text{BCS}}(0) = \lambda_L(0)\sqrt{1 + \xi_0/\ell} > \lambda_L(0)$  in the local limit [52, 53], where  $\xi_0 = \hbar v_F / (\pi \Delta_0)$  is the Pippard coherence length for pure superconductors ( $v_F = \hbar k_F / m^*$  is the Fermi velocity and  $\Delta_0$  is the BCS gap) [54]. From this  $\lambda_{\text{BCS}}(0)$  we calculate the superfluid density  $n_s^{\text{BCS}}(\ell)$ , which gives the disorder-induced suppression of  $n_s$  for a conventional BCS superconductor.

Figure 4(b) shows the comparison of the  $\ell$  dependences of  $n_s^{\text{exp}}$  and  $n_s^{\text{BCS}}$  ( $k_F \ell$  value is shown in the upper axis). In this figure, the BCS calculation is shown as a solid line and the inset shows the saturation of  $n_s^{\text{BCS}} \rightarrow 1$  in the clean limit  $\ell \rightarrow \infty$ . Clearly,  $n_s^{\text{exp}}$  does not agree with  $n_s^{\text{BCS}}$ ; although both are suppressed with decreasing  $\ell$ , the suppression is much stronger in  $\text{Cu}_x\text{Bi}_2\text{Se}_3$  than is expected for a BCS superconductor. Also, it is useful to compare the result shown in Fig. 4(b) to that in Fig. 1(b): At  $x > 0.3$ , the residual resistivity starts to increase drastically and  $\ell$  becomes shorter than  $\sim 25$  nm; however,  $n_s^{\text{exp}}$  tends to saturate in this dirtier range of  $\ell < 25$  nm. Moreover, for  $\ell < 4$  nm,  $n_s^{\text{exp}}$  intersects the  $n_s^{\text{BCS}}$  curve.

Hence, both the strong suppression in the intermediate disorder regime and the saturation tendency in the dirtier regime are anomalous. Such an anomalous behavior of  $n_s/n$  is the main result of this work, and it naturally points to an unconventional pairing state in  $\text{Cu}_x\text{Bi}_2\text{Se}_3$ .

In contrast to the highly anomalous behavior of  $n_s^{\text{exp}}$ , the modest suppression of  $T_c$  shown in Fig. 4(c) resembles the behavior of dirty conventional superconductors [35]. One might hasten to conclude that such an ordinary disorder dependence of  $T_c$  speaks against the odd-parity pairing, because the common belief for odd-parity superconductors is that  $T_c$  is quickly suppressed with impurity-induced disorder [31, 32]. However, as we already mentioned in the introduction, the particular type of odd-parity pairing that is considered to be realized in  $\text{Cu}_x\text{Bi}_2\text{Se}_3$  [9, 10] belies this common belief. This point was recently shown by Michaeli and Fu [23], who analyzed the novel inter-orbital, odd parity state proposed for  $\text{Cu}_x\text{Bi}_2\text{Se}_3$  [9]. The odd-parity pairing takes place between two  $p_z$  orbitals with different parity at the upper and lower ends of the quintuple layers via attractive short-range interactions. In such a state, the crucial disorder-induced pair breaking effect is significantly suppressed as a result of strong spin-momentum locking. The dephasing rate of the Cooper pairs depends on the ratio of band mass and chemical potential,  $m/\mu$ ; as this ratio becomes smaller, the superconductivity becomes more robust. For  $\text{Cu}_x\text{Bi}_2\text{Se}_3$ , this ratio has been estimated to be  $\sim 1/3$  [19] and the calculated  $T_c$  depends only weakly on the impurity-induced disorder [23], in qualitative agreement with Fig. 4(c). Therefore, the observed disorder effect in  $T_c$  is not inconsistent with the odd-parity pairing.

To summarize, we report an anomalous suppression of the superfluid density  $n_s/n$  probed by the lower critical field as a function of the Cu content  $x$ . Since the main effect of Cu intercalation beyond  $x \sim 0.3$  is to enhance disorder without changing band structure or carrier density, our result reveals the impact of disorder on the superconducting state in  $\text{Cu}_x\text{Bi}_2\text{Se}_3$ . Most strikingly, in the intermediate range of disorder,  $n_s/n$  is much more strongly suppressed than is expected for a dirty conventional BCS superconductor, while in the strongly disordered regime  $n_s/n$  tends to saturate. In contrast, the occurrence of superconductivity itself is robust against disorder as indicated by an only moderate suppression of  $T_c$  with  $x$ . The obviously anomalous behavior in  $n_s/n$  points to an unconventional pairing state, and the ostensibly normal behavior in  $T_c$  is consistent with the odd-parity pairing state with strong spin-momentum locking. Altogether, our result gives further support to the novel odd-parity pairing state in  $\text{Cu}_x\text{Bi}_2\text{Se}_3$ .

We thank L. Fu and Y. Tanaka for fruitful discussions, and S. Wada for technical assistance. This work was supported by JSPS (NEXT Program), MEXT (Innovative Area “Topological Quantum Phenomena” KAK-

ENHI 22103004), and AFOSR (AOARD 124038).

- 
- [1] L. Fu and C. L. Kane, Phys. Rev. Lett. **100**, 096407 (2008).
  - [2] A. P. Schnyder, S. Ryu, A. Furusaki, and A. W. W. Ludwig, Phys. Rev. B **78**, 195125 (2008).
  - [3] X.-L. Qi, T. L. Hughes, S. Raghu, and S.-C. Zhang, Phys. Rev. Lett. **102**, 187001 (2009).
  - [4] X.-L. Qi, T. L. Hughes, and S.-C. Zhang, Phys. Rev. B **81**, 134508 (2010).
  - [5] J. Linder, Y. Tanaka, T. Yokoyama, A. Sudbø, and N. Nagaosa, Phys. Rev. Lett. **104**, 067001 (2010).
  - [6] M. Sato, Phys. Rev. B **81**, 220504(R) (2010).
  - [7] X.-L. Qi and S.-C. Zhang, Rev. Mod. Phys. **83**, 1057 (2011).
  - [8] F. Wilczek, Nature Phys. **5**, 614 (2009).
  - [9] L. Fu and E. Berg, Phys. Rev. Lett. **105**, 097001 (2010).
  - [10] S. Sasaki, M. Kriener, K. Segawa, K. Yada, Y. Tanaka, M. Sato, and Y. Ando, Phys. Rev. Lett. **107**, 217001 (2011).
  - [11] Y. S. Hor, A. J. Williams, J. G. Checkelsky, P. Roushan, J. Seo, Q. Xu, H. W. Zandbergen, A. Yazdani, N. P. Ong, and R. J. Cava, Phys. Rev. Lett. **104**, 057001 (2010).
  - [12] L. A. Wray, S.-Y. Xu, Y. Xia, Y. S. Hor, D. Qian, A. V. Fedorov, H. Lin, A. Bansil, R. J. Cava, and M. Z. Hasan, Nature Physics **6**, 855 (2010).
  - [13] P. Das, Y. Suzuki, M. Tachiki, and K. Kadowaki, Phys. Rev. B **83**, 220513(R) (2011). In this paper the authors argue that a magnetic field created inside a vortex leads to a polarization of the spins forming the spin-triplet pairs in  $\text{Cu}_x\text{Bi}_2\text{Se}_3$  and hence a nonuniform spin magnetization in the sample. This is in contradiction to the non-magnetic, time-reversal-invariant pairing state discussed for  $\text{Cu}_x\text{Bi}_2\text{Se}_3$ , which consists of Cooper pairs with zero total angular momentum, see Refs. [9] and [19].
  - [14] L. Hao and T.K. Lee, Phys. Rev. B **83**, 134516 (2011).
  - [15] Y. Ishida, H. Kanto, A. Kikkawa, Y. Taguchi, Y. Ito, Y. Ota, K. Okazaki, W. Malaeb, M. Mulazzi, M. Okawa, S. Watanabe, C.-T. Chen, M. Kim, C. Bell, Y. Kozuka, H.Y. Hwang, Y. Tokura, and S. Shin, Phys. Rev. Lett. **107**, 077601 (2011).
  - [16] T. Kirzhner, E. Lahoud, K. B. Chaska, Z. Salman, and A. Kanigel, arXiv:1111.5805v1 (2011).
  - [17] M. Kriener, K. Segawa, Z. Ren, S. Sasaki, and Y. Ando, Phys. Rev. Lett. **106**, 127004 (2011).
  - [18] M. Kriener, K. Segawa, Z. Ren, S. Sasaki, S. Wada, S. Kuwabata, and Y. Ando, Phys. Rev. B **84**, 054513 (2011).
  - [19] L. A. Wray, S. Xu, Y. Xia, D. Qian, A. V. Fedorov, H. Lin, A. Bansil, L. Fu, Y.S. Hor, R. J. Cava, and M. Z. Hasan, Phys. Rev. B **83**, 224516 (2011).
  - [20] T. V. Bay, T. Naka, Y. K. Huang, H. Luigjes, M. S. Golden, and A. de Visser, Phys. Rev. Lett. **108**, 057001 (2012).
  - [21] C. W. J. Beenakker, arXiv:1112.1950v2 (2012).
  - [22] T. H. Hsieh and L. Fu, Phys. Rev. Lett. **108**, 107005 (2012).
  - [23] K. Michaeli and L. Fu, arXiv:1203.1055v1 (2012).
  - [24] Y. Tanaka, M. Sato, and N. Nagaosa, J. Phys. Soc. Jpn. **81**, 011013 (2012).
  - [25] Y. Tanaka, K. Nakayama, S. Souma, T. Sato, N. Xu, P. Zhang, P. Richard, H. Ding, Y. Suzuki, P. Das,



- K. Kadowaki, and T. Takahashi, Phys. Rev. B **85**, 125111 (2012).
- [26] A. Yamakage, K. Yada, M. Sato, and Y. Tanaka, Phys. Rev. B **85**, 180509(R) (2012).
- [27] Y. Tanaka and S. Kashiwaya, Phys. Rev. Lett. **74**, 3451 (1995).
- [28] S. Kashiwaya and Y. Tanaka, Rep. Prog. Phys. **63**, 1641 (2000).
- [29] H.-J. Zhang, C.-X. Liu, X.-L. Qi, X.-Y. Deng, X. Dai, S.-C. Zhang, and Z. Fang, Phys. Rev. B **80**, 085307 (2009).
- [30] C.-X. Liu, X.-L. Qi, H.J. Zhang, X. Dai, Z. Fang, and S.-C. Zhang, Phys. Rev. B **82**, 045122 (2010).
- [31] R. Balian and N. R. Werthamer, Phys. Rev. **131**, 1553 (1963).
- [32] A. I. Larkin, Sov. Phys. JETP Lett. **92**, 130 (1965).
- [33] A. P. Mackenzie and Y. Maeno, Rev. Mod. Phys. **75**, 657 (2003).
- [34] Y. Maeno, S. Kittaka, T. Nomura, S. Yonezawa, and K. Ishida, J. Phys. Soc. Jpn. **81**, 011009 (2012).
- [35] P. W. Anderson, J. Phys. Chem. Solids **11**, 26 (1959).
- [36] The magnetization was measured at several temperatures between 1.8 K and  $T_c$  of each sample. Before each run, the sample temperature was stabilized at 5 K ( $> T_c$ ) and the magnet was quenched to remove any remnant field. Then the sample was cooled in zero field to the desired temperature and the magnetization was measured with increasing magnetic field.
- [37] R. A. Klemm, J. Low Temp. Phys. **39**, 589 (1980).
- [38] V. G. Kogan, Phys. Rev. B **24**, 1572 (1981).
- [39] J. R. Clem, Physica C **162**, 1137 (1989).
- [40] A. L. Fetter and P. C. Hohenberg in *Superconductivity*, edited by R. D. Parks (Marcel Dekker, New York, 1969), Vol. 2, Chap. 14.
- [41] A. A. Abrikosov, Sov. Phys. JETP **5**, 1174 (1957).
- [42] C.-R. Hu, Phys. Rev. B **6**, 1756 (1972).
- [43] R. Liang, D. A. Bonn, W. N. Hardy, and D. Broun, Phys. Rev. Lett. **94**, 117001 (2005).
- [44] The effective mass  $m^*$  was estimated for  $x = 0.29$  from normal-state specific-heat data [17] to be  $m^* = 2.6m_e$  ( $m_e$  is the bare electron mass).
- [45] E. H. Brandt, Phys. Rev. B **60**, 11939 (1999).
- [46] M. Ma and P.A. Lee, Phys. Rev. B **32**, 5658 (1985).
- [47] A. V. Balatsky, I. Vekhter, and J.-X. Zhu, Rev. Mod. Phys. **78**, 373 (2006).
- [48] J. L. Tallon, J. R. Cooper, S. H. Naqib, and J. W. Loram, Phys. Rev. B **73**, 180504(R) (2006).
- [49] W. DeSorbo, Phys. Rev. **132**, 107 (1963).
- [50] C. Egloff, A. K. Raychaudhuri, and L. Rinderer, J. Low Temp. Phys. **52**, 163 (1983).
- [51] Although the disorder increases with  $x$ ,  $k_F\ell$  is still much larger than 1 and hence  $\text{Cu}_x\text{Bi}_2\text{Se}_3$  is in the weakly disordered regime [46, 47]. Also, the ratio  $\xi_0/\ell$  is about 1 for  $x \approx 0.26$  and hence  $\text{Cu}_x\text{Bi}_2\text{Se}_3$  is in-between the clean and dirty limits.
- [52] A. K. Raychaudhuri, C. Egloff, and L. Rinderer, J. Low Temp. Phys. **53**, 513 (1983).
- [53] M. Tinkham, *Introduction to Superconductivity* (McGraw-Hill, New York, 2nd edition, 1996), Chap. 3.10.4.
- [54] For our calculation of  $\lambda_{\text{BCS}}(0)$  expected for BCS superconductors, we used the BCS gap value  $\Delta_0 = 1.764 k_B T_c^0$  with the clean-limit critical temperature  $T_c^0$  which we identify with the maximum  $T_c$  of 3.8 K in  $\text{Cu}_x\text{Bi}_2\text{Se}_3$ .